Maturation and phenotype of pathophysiological neuronal excitability of human cells in tau-related dementia

Olga Kopach[1,*], Noemí Esteras[2], Selina Wray[3], Dmitri A. Rusakov[1], Andrey Y. Abramov[2,*]

[1]Department of Clinical and Experimental Epilepsy, UCL Queen Square Institute of Neurology, London, UK
[2]Department of Clinical and Movement Neurosciences, UCL Queen Square Institute of Neurology, London, UK
[3]Department of Neurodegenerative Disease, UCL Queen Square Institute of Neurology, London, UK

[*] Correspondence
Dr Olga Kopach, Department of Clinical and Experimental Epilepsy, UCL Queen Square Institute of Neurology, Queen Square, WC1N 3BG, London, UK
Email: o.kopach@ucl.ac.uk
Prof. Andrey Y. Abramov, Department of Clinical and Movement Neurosciences, UCL Queen Square Institute of Neurology, Queen Square, WC1N 3BG, London, UK
Email: a.abramov@ucl.ac.uk

Keywords: tau pathology; human cells; maturation of iPSC-derived neurons; neuronal excitability; neuropathological phenotype; frontotemporal dementia and parkinsonism.

JCS Advance Online Article. Posted on 16 April 2020

Summary statement

The pathophysiological excitability was revealed for human cells in dementia. This provides a major advance in understanding of tau-induced brain neuropathology and sheds new light on human models of dementia.

Abstract

Frontotemporal dementia and parkinsonism (FTDP-17) caused by the 10+16 splice-site mutation in the *MAPT* provides an established platform to model tau-related dementia *in vitro*. Human iPSC-derived neurons have been shown to recapitulate the neurodevelopmental profile of tau pathology during *in vitro* corticogenesis as in the adult human brain. However, the neurophysiological phenotype of these cells has remained unknown, leaving unanswered questions over the functional relevance and the gnostic power of this disease model. Here we used electrophysiology to explore the membrane properties and intrinsic excitability of the generated neurons to find that human cells mature by ~150 days of neurogenesis to become compatible with matured cortical neurons. In earlier FTDP-17, neurons, however, exhibited a depolarized resting membrane potential associated with increased resistance and reduced voltage-gated Na^+- and K^+-channel-mediated conductance. The $Na_v1.6$ protein was reduced in FTDP-17. These led to a reduced cell capability of induced firing and changed action potential waveform in FTDP-17. The revealed neuropathology may thus contribute to the clinicopathological profile of the disease. This sheds new light on the significance of human models of dementia *in vitro*.

Introduction

A recurrent problem in dementia research is that the generated animal models do not show neuropathological profiles that match pathological changes found in the human brain (Van Dam and De Deyn, 2006, Irwin et al., 2018, Rohrer et al., 2011, Gotz and Ittner, 2008). While the wide use of animal models (~180 models of Alzheimer's disease are currently available) remains under scrutiny, the latest advances in generating patient-specific nerve cells from induced pluripotent stem cells (iPSC) have enabled studies in live human cells (Livesey, 2014, Shi et al., 2012b). Because such model systems are ideally suited for exploring the mechanistic basis of cellular pathogenesis in live cells, they could provide an essential tool for exploring the cell and molecular biology of dementia (Iovino et al., 2015, Ortiz-Virumbrales et al., 2017, Sposito et al., 2015).

Various types of dementia share common functional impairments that occur in nerve cells as the disease progresses. This suggests that different dementia forms have a similar cellular basis. As an example, a class of tauopathies that includes, among others, Alzheimer's disease, Pick's disease, the inherited frontotemporal dementia and parkinsonism linked to chromosome 17 (FTDP-17), has featured the abnormal tau protein, which appears to underlie the pathology at the neuronal level. The primary molecular mechanism involving a self-aggregation of hyperphosphorylated tau includes toxicity of the tau deposits, and eventually neuronal death in Alzheimer's disease (Goedert et al., 1989, Matsuo et al., 1994) and FTDP-17 (Hutton et al., 1998, Pickering-Brown et al., 2002, Poorkaj et al., 1998). However, how exactly tau pathology affects human nerve cell function leading to cell death remains unknown for the whole class of tauopathies.

We therefore sought to understand changes, if any, in the neurophysiological properties of human cells in tau-related dementia, in particular, in a human iPSC model of FTDP-17 caused by the 10+16 intronic mutation in the gene coding the microtubule-associated protein tau (*MAPT*). This experimental model recapitulates the developmental changes in tau-splicing pathology (increased splicing of 4R tau isoforms) as found in the adult human brain (Sposito et al., 2015, Verheyen et al., 2018, Paonessa et al., 2019). Because very little is known about neurophysiology of human cells with tau pathology at any stage of earlier or overt symptoms, we sought to establish firstly the timeline of functional neuronal maturation *in vitro*. Having established the timing of well-developed neurophysiological properties of human iPSC-derived neurons in control (healthy donor iPSC lines), we next examined the

biophysical properties of neurons with the 10+16 *MAPT* mutation to document the pathophysiological phenotype of intrinsic excitability for human cells in FTDP-17.

Results

Time-dependent maturation of intrinsic excitability of human iPSC-derived cortical neurons

Human iPSC-derived cells were positively stained for several cortical layers neuronal markers, detectable following 80 days of *in vitro* neurogenesis in control lines (healthy donors) and those obtained from patients with FTDP-17 caused by the 10+16 intronic mutation in *MAPT* (Sposito et al., 2015). Consistently, cells displayed a clear neuronal morphology at 100 days of corticogenesis in these cell lines (Fig. 1A). Hence, patch-clamp recordings were performed from iPSC-derived neurons to trace the maturation of their biophysical properties over an extended period of neurogenesis – at 100 and 150 DIV – for the anticipated neurophysiological maturation of the differentiated neurons. At this developmental stage, iPSC-derived neurons with the mutation express both 3R and 4R tau isoforms, while control cells only the 3R tau isoform (Sposito et al., 2015).

Intrinsic membrane properties determine key aspects of neuronal function and behaviour. We, therefore, started by comparing the passive membrane properties of the generated cells between different time-points in control lines. Firstly, there was a substantial increase in the membrane capacitance (C_m) – an almost twofold – between 100 and 150 DIV (from 29.6 ± 2.6 pF, n = 17 to 61.0 ± 6.9 pF, n = 37, respectively, $p < 0.001$; Fig. 1B). Secondly, other passive properties of the membrane, such as the input resistance (R_{in}, indicating membrane conductance – a pool of readily available functional ion channels) and the time constant (τ_m, referring to the time for neuron's membrane potential to reach 63% of its resting value) were also markedly improved by the age of ~150 DIV (R_{in}, 196.5 ± 33.4 MΩ, n = 17 vs. 690.2 ± 90.9 MΩ, n = 37, $p < 0.001$ at 100 and 150 DIV, respectively; τ_m, 5.6 ± 1.0 ms, n = 17 vs. 43.4 ± 5.5 ms, n = 37, $p < 0.001$, respectively; Figs 4B and 4C). Thirdly, we measured the resting membrane potential (V_{rest}, immediately after membrane breakthrough). At 100 DIV, V_{rest} was relatively depolarized, as observed in all tested cells (a range from −17 mV to −32 mV, an average of −25.3 ± 1.8 mV, n = 10; Fig. 1C). This suggests that the generated neurons at this developmental age remain underdeveloped. Indeed, only a proportion of iPSC-derived neurons at the

age of 100 DIV (6 out of 18) enabled generating a single action potential (AP) in response to current injection (V_{rest} held at −60 mV to −70 mV; Fig. 1D). We never observed a cell capable of generating a train of induced APs at 100 DIV. The V_{rest} markedly developed by ~150 DIV (a range from −43 mV to −70 mV, average −54.7 ± 2. 5 mV, n = 23; Fig. 1C). Consistent with the 'maturation' of V_{rest}, neurons developed their capability for a high-frequency discharge (Fig. 1D).

Next, we assessed the voltage-dependent membrane properties underlying the intrinsic excitability of differentiated cells. Because the hyperpolarization-activated cation current (I_h), a mixed current carried by both K^+ and Na^+, makes an important contribution to setting of the V_{rest} (Biel et al., 2009, Ludwig et al., 1998), hence reflects a maturation level, we measured cell responses to hyperpolarizing current steps. For quantitative comparisons, we calculated the V_{drop} and the sag response (the ratio of the peak to steady-state) for the hyperpolarizing current pulse of −150 pA (Fig. 2A). The iPSC-derived neurons showed a much prominent V_{drop} at 150 DIV than at 100 DIV (120.9 ± 14.0 mV, n = 18 vs. 46.3 ± 12.6 mV, n = 17, respectively, p < 0.001; Fig. 2B). In line with this, neurons at the age of 150 DIV exhibited the larger voltage sag, which followed in some cells by a rebound spike on termination of the hyperpolarization step (Fig. 2A), while cells at 100 DIV had a minor or no sag response (0.31 ± 0.05 vs. 0.10 ± 0.04, respectively, p < 0.01; Fig. 2B). Since HCN channels largely mediate I_h (Bennett et al., 2000, Biel et al., 2009), the increased I_h (three-fold increase in the sag ratio) indicates an increased HCN channel density by ~150 DIV (improved neuronal maturation).

To assess the functional expression of fast-activating Na^+ channels underlying cell firing activity, we next examined the AP upstroke in the generated neurons (Fig. 2C). Further to a cell's capability of generating a train of induced APs at 150 DIV (as compared to a generated single AP spike by iPSC-derived neurons at 100 DIV; Figs 1D, 2C left traces), the AP spike was of a larger amplitude at 150 DIV (Fig. 2C right). Importantly, the AP threshold has further developed, as revealed by an analysis of the first AP in a train induced by a slow-injecting ramp current (−20.9 ± 6.4 mV at 100 DIV vs. −42.9 ± 2.0 mV at 150 DIV, n = 9, p < 0.05; Fig. 2D), that the threshold became thus comparable to that of primary brain neurons (Kopach et al., 2018b, Kopach et al., 2018a). The slow after-hyperpolarization (sAHP) mediated by K^+-channels which largely contribute to AP repolarization and spike shaping (Wilson and Goldberg, 2006) was also developed. The sAHP, measured at the end of a square depolarizing pulse train (Fig. 2C), markedly increased by ~150 DIV, with a clear

difference between ~100 and ~150 DIV detectable for all depolarizing currents tested, including relatively small currents (a range of 0 to 450 pA; Fig. 2E). This reflects a time-dependent increase in the K^+-channel density, especially Ca^{2+}-activated K^+-channel subtypes, as an ionic basis of the sAHP component in pyramidal neurons (Andrade et al., 2012, King et al., 2015).

Altogether, human iPSC-derived cortical neurons require ~150 DIV to mature intrinsic excitability up to a common neurophysiological level.

Human iPSC-derived neurons with the *MAPT* mutation display normal development but changed intrinsic excitability

Having established the time of maturation of neurophysiological excitability for control human cells (non-demented group) as ~150 DIV, we next investigated the intrinsic excitability of cells with the 10+16 intronic mutation in *MAPT* (FTDP-17 group).

Firstly, we assessed iPSC-derived neurons with the mutation for their morphological development at an earlier stage of corticogenesis, at ~100 DIV. For the analysis of neuronal morphology, cells were immunostained for β-tubulin III and GFAP, together with nuclear staining, and two parameters of the area and the diameter of neuronal somata were both quantified in control and FTDP-17 lines (Fig. 3A). We analyzed a total of 367 neurons derived from the two control lines and 431 neurons derived from iPSC lines obtained from two FTDP-17 patients with the 10+16 *MAPT* mutation (at least 6 independent preparations per group tested). The quantitative analysis of the neuronal somata area revealed a similar distribution in the density (number of cells) between pooled control and FTDP-17 groups (Fig. 3B). Similarly, the soma diameter did not also differ between the groups (median, ~8.8 μm in control and ~8.3 μm in FTDP-17, $p = 0.359$ Mood's median test; Fig. 3C). These results demonstrate that human cells with the mutation develop neuronal morphology to a similar extent as control ones at the age of ~100 DIV.

Secondly, we made patch-clamp recordings from the iPSC-derived neurons with the mutation. In full agreement with morphological assessment, electrophysiological studies showed no significant difference in the C_m of iPSC-derived neurons in FTDP-17, as compared to the age-matching control at 100 DIV, but a trend to increase in FTDP-17 (29.6 ± 2.6 pF, n = 17 in control vs. 44.6 ± 9.6 pF, n = 7 in FTDP-17, $p = 0.175$; Fig. 4A). Neither was observed over an extended period of neurogenesis, at 150 DIV, regardless of comparison between the pooled groups (61.0 ± 6.9 pF, n = 37 in control vs. 60.3 ± 5.1 pF, n = 66 in FTDP-17, $p = 0.935$; Fig.

4A left) or *per* individual case (median, ~43.3 pF, n = 37 control neurons vs. ~45.6 pF, n = 31 neurons from patient 1, $p = 0.667$ vs. ~52.73, n = 34 neurons from patient 2, $p = 0.797$, Mann-Whitney test; Fig. 4A right).

Thirdly, one of the other passive properties of membrane, τ_m, did not also change in neurons between FTDP-17 and the age-matched control at any time-point tested. The τ_m was 5.6 ± 1.0 ms (n = 17) in control vs. 13.9 ± 4.5 ms (n = 7, $p = 0.120$) in FTDP-17 at 100 DIV and 43.4 ± 5.5 ms (n = 37) vs. 46.2 ± 3.7 ms (n = 66, $p = 0.665$), respectively, at 150 DIV (Fig. 4B). Collectively, this suggests a 'normal' development of iPSC-derived neurons with the 10+16 mutation in *MAPT* (i.e. similar to the age-matched control) over the examined period of neurogenesis.

However, neurons with the mutation exhibited changed membrane excitability by ~150 DIV. In comparison to control group, neurons with the mutation had an increased R_{in} (690.2 ± 90.9 MΩ, n = 37 in control vs. 1000.6 ± 112.7 MΩ, n = 66 in FTDP-17, $p < 0.05$; Fig. 4C), although no difference was found at the age of 100 DIV (196.5 ± 33.4 MΩ, n = 17 in control vs. 270.7 ± 42.3 MΩ, n = 7 in FTDP-17, $p = 0.190$; Fig. 4C). Further, neurons with the mutation displayed a depolarized V_{rest} at 150 DIV, as compared to the age-matched control (Fig. 4D), significant for each individual case (median value, –53 mV, n = 23 in control vs. –39.0 mV, n = 22, patient 1, $p < 0.001$ and vs. –41.5 mV, n = 24, patient 2, $p < 0.001$, Mann-Whitney test; Fig. 4D). Again, such a depolarized V_{rest} could not be due to a slower V_{rest} maturation in neurons with the mutation because at 100 DIV these cells developed their V_{rest} even more hyperpolarized than control cells (−25.3 ± 1.8 mV, n = 10 in control vs. −45.9 ± 7.0 mV, n = 5 in FTDP-17, $p < 0.05$; Fig. 4D left).

To assess whether such an increase in membrane excitability of human cells in FTDP-17 could be due to impairments in the voltage-dependent conductance mediated by HCN channels, we recorded the I_h. Surprisingly, there was no significant difference in the I_h between control and FTDP-17 at 150 DIV (V_{drop}, n = 17 in control and n = 32 in FTDP-17, $p = 0.190$; the sag ratio, n = 16 and 32, respectively, $p = 0.798$, Mann-Whitney test; Fig. 5A), nor at 100 DIV (V_{drop}, n = 17 in control and n = 6 in FTDP-17, $p = 0.403$; the sag ratio, n = 17 in control and n = 6 in FTDP-17, $p = 0.806$; Fig. 5A). Western-blot analysis further confirmed a similar level of the HCN1 protein expression between control and neurons with the *MAPT* mutation at ~150 DIV (Fig. 5B). This suggests that other voltage-gated conductance, instead of HCN channels, is to be involved in an increased membrane excitability of neurons with the *MAPT* mutation by the age of ~150 DIV.

Functional down-regulation of voltage-gated Na^+- and K^+-channels in human cells with tau pathology: implication of neuronal $Na_v1.6$ channel in FTDP-17

We next asked whether the voltage-gated membrane conductance mediated by Na^+- and K^+-channels could be affected in human cells by the mutation in *MAPT*. To assess this, we recorded Na^+- (I_{Na}) and K^+-currents (I_K) in differentiated neurons at 150 DIV at different membrane potentials and plotted the current-voltage (*I-V*) relationships for both channels to compare between control and FTDP-17. A majority of recorded cells displayed the robust voltage-activated I_{Na} and I_K (Fig. 6A). The *I–V* relationship showed that I_{Na} activation occurs at a range of membrane potentials more positive than approximately –50 mV, with no bias in the *I–V* curve shape, but a clear reduction in the I_{Na} density in neurons with the mutation (n = 12 in control and n = 36 in FTDP-17; Fig. 6B). The peak of I_{Na} density was dramatically decreased in cells with the mutation (median, ~7.39 pA/pF in control vs. ~1.9 pA/pF in FTDP-17, $p < 0.05$ Mann-Whitney test; Fig. 6B). Also, there was a decrease in the density of I_K (consisting of fast and slow non-inactivating components) in FTDP-17 – the reduction appeared at membrane potentials more positive than –30 mV (n = 7 in control and n = 30 in FTDP-17; Fig. 6C). This indicates the functional down-regulation of Na^+- and K^+-channels in FTDP-17.

To evaluate the mechanism for tau-related functional down-regulation of Na^+-channels, we examined the protein expression in iPSC-derived neurons in control and FTDP-17 at 130-165 DIV. Western blot experiments demonstrated the reduced expression of $Na_v1.6$ channel in neurons with the mutation (n = 6 samples in control and n = 8 in FTDP-17, 4 independent experiments performed, $p < 0.05$ Mann-Whitney test; Fig. 6D). This indicates a loss of neuronal $Na_v1.6$ channel as a mechanism contributing to changed intrinsic excitability of human cells in FTDP-17.

Since voltage-gated Na^+- and K^+-channels are largely responsible for neuronal firing, functional down-regulation of these channels would lead to impaired cell function – changes in firing activity. Therefore, we examined changes in AP discharge by neurons with the mutation at 150 DIV, using two different experimental protocols: eliciting firing by injecting a slow ramp current (200 pA/s; Fig. 7A) and by injecting a series of short, square depolarizing pulses (Fig. 7C). Firstly, we found that neurons with the mutation exhibited a depolarized AP threshold (measured for the first AP spike in a train elicited by a ramp protocol), as compared to that in age-matched control neurons (−42.4 ± 2.3 mV, n = 4 in control vs. −31.1 ± 2.6 mV, n = 9

in FTDP-17, $p < 0.05$; Fig. 7A). Thus, a shift in the threshold was by ~11 mV (depolarizing shift). Secondly, there was a reduction in the amplitude of induced AP spike (from 46.9 ± 2.9 mV, n = 14 in control to 35.5 ± 2.5 mV, n = 36 in FTDP-17, $p < 0.05$; Fig. 7B). Thirdly, neurons with the mutation exhibited an increased rheobase – the magnitude of depolarizing current required to shift membrane potential to the spike threshold to drive firing (Fig. 7C). The two-fold stronger current was needed to bring neurons with tau pathology to firing (96.1 ± 11.5 pA, n = 41 whereas in control neurons current sufficient to elicit firing was on average of 48.2 ± 8.2 pA, n = 11, $p < 0.05$; Fig. 7C). The latter indicates that neurons with tau pathology need near a twice stronger stimulus to drive firing. Finally, neurons with the mutation had a decreased sAHP, as observed at different depolarizing current pulses (50 to 250 pA; Fig. 7D), consistent with a reduced K^+-channel density in these neurons. Overall, these changes attribute to the phenotypic spectrum of pathological neuronal excitability of human cells in FTDP-17.

Discussion

Human stem cell models that employ patient-specific cell types have been a milestone in dementia research. However, physiological studies of iPSC-derived neurons are challenging and sparse. Here, we show that human iPSC-derived cortical neurons require ~150 days of neurogenesis to match the physiological traits of mature cortical neurons. For the first time, we reveal the phenotypic pathophysiological intrinsic excitability of human cells in frontotemporal dementia and parkinsonism related to tau protein pathology.

Maturation of neurophysiological properties of human cells *in vitro*

Despite that dementia is a disorder gradually progressing over a considerably prolonged time, at present, there is no precise treatment to cease or modify the disease. The major challenge in developing therapies has been the lack of a clear understanding of the mechanistic basis underlying the neuropathology. Since animal models appear to not fully replicate neuronal loss as it occurs in the human brain being associated with a clear clinicopathological profile of memory loss and cognitive decline (as somewhat debatable for animal species), human stem cell models have been implicated to modelling genetic forms of Alzheimer- and non-Alzheimer-type dementias for the studies of patient-specific cells directly. This study provides the

electrophysiological expertise of human iPSC-derived cortical neurons to establish, in the first instance, neuronal maturation of human cells in control and FTDP-17 with tau pathology.

The timing of iPSC-derived neurons mature and set neurophysiological activity has always been a challenge that most studies overcome via routine use of various antigens/markers. Whereas immunocyto(histo)chemistry can document a firm expression of receptors/proteins in generated nerve cells, it won't prove the cell function, with regard to a constitutive level of neurophysiological activity (Kopach, 2019). To the neurophysiological point of view, the biophysical properties of human iPSC-derived cortical neurons at 150 days of neurogenesis in control (non-demented cell lines) confirm these cells are physiologically credible. The matured intrinsic excitability of generated neurons was confirmed cumulatively by their V_{rest} and the AP threshold – both comparable to that of primary brain neurons (Kopach et al., 2018b) – and a cell capability of high-frequency firing by the age of ~150 DIV. In comparison to control, neurons with the mutation in *MAPT* (demented group) did not appear to have the underdeveloped biophysical properties when being examined at the age of 100 DIV, nor at 150 DIV. For instance, the I_h (reflecting the functional HCN channel expression responsible for the recovery from hyperpolarization) was comparable to that in control neurons, consistently with a similar level of HCN1 protein expression (Fig. 5). Likewise, some of the passive membrane properties, such as the capacitance and the time constant were also similar between the groups (Fig. 4). Quantification of neuronal morphology (the somata size) further confirmed neuronal development to a similar extend between the groups, using a different to electrophysiology approach (Fig. 3).

Overall, varied tests (quantitative comparison of morphological or electrophysiological parameters) indicate that human iPSC-derived neurons mature intrinsic excitability to a constitutive neurophysiological level by ~150 days of corticogenesis, in control and FTDP-17 cell lines.

Pathophysiological neuronal excitability of human cells in FTDP-17

The established biophysical properties of the generated neurons suggest the reliable model use for functional studies of genetic forms of tauopathy. In this stem cell model, the developmental changes in tau splicing pathology have been already confirmed (Paonessa et al., 2019, Sposito et al., 2015, Iovino et al., 2015), detecting both 3R and 4R adult brain tau isoforms after a few months of *in vitro* corticogenesis

in FTDP-17 while only 3R in control (non-demented) cell lines. This study documents the tau-related neuropathological phenotype of human cell function through detecting the pathophysiological intrinsic excitability of neurons with the mutation at the development stage between ~100 and 150 DIV. The phenotype could be described by i) a depolarized V_{rest}, ii) an increased R_{in}, iii) a downregulated Na^+- and K^+-channel-mediated conductance, leading to iv) functional impairments in firing activity and v) changed waveform of APs in FTDP-17. At this earlier stage of the pathology, cells exhibited a depolarized AP threshold (depolarizing shift in ~11 mV) and generated APs of a smaller amplitude and altered shape, and displayed a reduced capability of induced firing (a near twice stronger stimulus needed to drive firing).

Numerous experimental studies showed the tau-related neuronal dysfunction using animal models, at either earlier or advanced stages of the pathology. It includes (but not limited to) a reduced firing of neocortical neurons reported in a transgenic model of tauopathy *in vivo* (Menkes-Caspi et al., 2015), frontotemporal dementia and amyotrophic lateral sclerosis (Radzicki et al., 2016), Alzheimer models (Busche et al., 2019) and parkinsonism (Fieblinger et al., 2014) that opposes neuronal hyperexcitability in aged animals (Crimins et al., 2012). The emerged discrepancy could relate to severe morphological impairments (regression of the brain structure) at later stages, i.e. the loss of synapses and cell death (Crimins et al., 2011) and, in general, to careful interpolation of obtained phenotypes in transgenic models by considering the important physiological role of tau in neuronal excitability (DeVos et al., 2013) and synaptic plasticity (Kimura et al., 2014) because tau overexpression would rapidly shift neurons to hyperexcitability.

The revealed phenotype of pathological neuronal excitability of human cells in FTDP-17 has emerged, at least partially, due to a loss-of-function of voltage-gated Na^+-channels, in particular neuronal $Na_v1.6$ channel as one of the predominant candidates. The role of $Na_v1.6$ channel in the AP initiation and propagation in cortical excitatory pyramidal neurons (Hu et al., 2009) implies the impaired AP parameters and firing discharge by neurons with the *MAPT* mutation. Dysfunction of $Na_v1.6$-mediated currents was associated with altered learning and memory, being linked to a number of neurological and psychiatric brain disorders, such as epilepsy, intellectual disability and sudden unexpected death in epilepsy (Estacion et al., 2014, Lopez-Santiago et al., 2017, Wagnon et al., 2017). Thus far, we have only revealed a reduced $Na_v1.6$ channel expression in FTDP-17, while other voltage-gated channels could also be involved in this neuropathology. For example, our data indicate that K^+-

channels are very like to contribute to the phenotypic pattern of human cell excitability in FTDP-17. Since the slow component of AHP that lasts hundreds of ms to seconds is Ca^{2+}-dependent (Azouz et al., 1996, Power et al., 2002), the reduced sAHP in FTDP-17 suggests a functional down-regulation of Ca^{2+}-dependent K^+-channels (Andrade et al., 2012, King et al., 2015) those mediate the AP repolarization (Azouz et al., 1996, King et al., 2015) and are essential for the generation of rhythmic bursts (Wilson and Goldberg, 2006). Taking into account that slowly inactivating, voltage-gated K^+-conductance could be mediated by several channel types, not limited to the Kv1, Kv2, Kv3, and Kv7 subfamilies, numerous candidates are to be considered at the moment as potential contributors to the pathophysiological excitability of human cells with the *MAPT* mutation. Most promising ones apparently refer to Kv1 subfamily (containing Kv1.1, Kv1.2, and Kv1.6) whose expression contributes to changed rheobase, AP threshold and the spike waveform (Wykes et al., 2012, Brew et al., 2003).

The tau-induced impairments in intrinsic neuronal excitability can be accompanied by changes in synaptic excitability. The abnormal synaptic function was observed in transgenic animal models before tau aggregates appeared (Van der Jeugd et al., 2012) and prior to neurodegeneration (Menkes-Caspi et al., 2015). Whether this phenotype of intrinsic neuronal excitability of human cells in FTDP-17 is associated with altered synaptic excitation (transmission) remains to be determined, to decipher in detail the tau-related changes in human cell function at the neuronal network level.

Altogether, this study provides evidence for the time-dependent maturation of neurophysiological properties of human iPSC-derived cortical neurons during *in vitro* neurogenesis, essential for the reliable model use in studies of tau-related dementia *in vitro*. The pathophysiological phenotype of intrinsic neuronal excitability of human cells with the 10+16 splice-site mutation in *MAPT* has been revealed at 150 DIV to provide a major advance in our understanding of human brain cell dysfunctions at earlier stages of tau-induced dementia. These findings shed new light on human stem cell models of dementia.

Materials and Methods

Human stem cell model of FTDP-17

This study included 4 human cell lines those two were control (non-demented) iPSC lines and two obtained from patients bearing the 10+16 *MAPT* mutation (FTDP-17 group). Human iPSC lines were as reported previously in detail (Esteras et al., 2017, Sposito et al., 2015). In particular, two 10+16 *MAPT* iPSC lines were generated by retroviral-transduction reprogramming of fibroblasts obtained from the National Hospital for Neurology and Neurosurgery (London, UK). One control iPSC line, also generated using retroviral transduction from fibroblasts, was obtained from the laboratory of Dr Kunath (Edinburgh University, UK). Another control was purchased from ThermoFisher Scientific. Human iPSC-derived neurons were generated and characterized as previously described (Shi et al., 2012a, Sposito et al., 2015, Esteras et al., 2017). Briefly, differentiation of the pluripotent stem cells into cortical neurons was performed via dual SMAD inhibition for ten days followed by an *in vitro* neurogenesis. Forty-sixty days after induction, cells were plated on poly-ornithine/laminin-coated glass coverslips and maintained until used in neural maintenance media, composed of a mixture of N2 and B27 media as described elsewhere (Shi et al., 2012a), with media changes twice a week.

For each group, at least 6 different preparations were examined. Patch-clamp experiments were performed by the experimenter in a blind to experimental group manner.

Immunocytochemistry

Immunocytochemistry was performed using a common immunostaining protocol by fixing neuronal cultures with 4% paraformalgehyde (15 min at room temperature), followed by permeabilization/blocking with 0.2% Triton X-100 and 10% bovine albumin serum (BSA) for 1 hour. Cells were then incubated with Alexa-Fluor®-conjugated primary antibodies (anti-β-tubulin III and anti-GFAP, 1:200, Abcam, UK) overnight at 4°C. Hoechst 33342 (10 μM) was used to stain nuclei. Confocal imaging was carried out using a Zeiss 710 VIS CLMS confocal microscope.

Western blot analysis

Cells were washed with PBS and lysed in an ice-cold RIPA lysis buffer supplemented with protease and phosphatase inhibitors (ThermoFisher, Paisley, UK). Samples were snap frozen, sonicated and centrifuged at 14000 rpm; the protein content was

determined by the Pierce™ BCA protein assay (ThermoFisher, Paisley, UK). Protein (20 µg) was fractionated on a SDS polyacrylamide gel (4-12%) (ThermoFisher, Paisley, UK), transferred to a PVDF membrane (Bio-Rad, Richmond, CA), and blocked with 5% non-fat milk. Membranes were incubated overnight with primary antibodies (HCN1 and $Na_v1.6$ 1:500, Alomone Labs, Jerusalem, Israel; β-actin 1:5000, Cell Signaling Technologies, MA, USA), diluted in 5% BSA; then with HRP-conjugated secondary antibodies. The luminol-based Pierce™ ECL Western Blotting Substrate (ThermoFisher Scientific) was used to detect the HRP activity. Protein band densities were quantified using ImageJ software (NIH, Maryland, USA) after scanning of the X-ray films, and normalized to control.

Whole-cell electrophysiology

Whole-cell recordings were made from iPSC-derived neurons (Fig. 1A), using Multipatch 700B amplifier controlled by pClamp 10.2 software package (Molecular Devices, USA). For the recordings, a neuronal culture was placed in a recording chamber mounted on the stage of Olympus BX51WI upright microscope (Olympus, Japan) equipped with a LUMPlanFI/IR 40×0.8 objective coupled to an infrared DIC imaging system. Recordings were performed in a bicarbonate-buffered solution (aCSF) containing (in mM) 126 NaCl, 3 KCl, 2 $MgSO_4$, 2 $CaCl_2$, 26 $NaHCO_3$, 1.25 NaH_2PO_4, 10 D-glucose (95% O_2 and 5% CO_2; pH 7.4; osmolarity 300–310 mOsmol) at 31–33°C. Recording electrodes had the resistance of 2.5-5 MΩ when filled with a K-gluconate-based intracellular solution containing (in mM) 126 K-gluconate, 10 HEPES, 4 KCl, 4 $MgCl_2$, 2 BAPTA, 4 Mg-ATP, 0.4 GTP-Na; pH 7.2 with KOH, osmolarity ~290 mOsmol). Once in the whole-cell, iPSC-derived neurons were recorded for passive membrane properties, including the resting membrane potential (V_{rest}), which was detected immediately after membrane breakthrough, the membrane capacitance (C_m), the input resistance (R_{in}), and the membrane time constant (τ_m), measured from the hyperpolarizing squire current pulse steps in current mode. The constant, measured as a function of two properties of membrane, R_m and C_m, was calculated from the equation: $\tau_m = R_m \cdot C_m$.

Experimental protocols and data analysis

For the assessment of intrinsic excitability, iPSC-derived neurons were tested in the first instance for their capability of generating induced AP. Neuronal firing was elicited using either of the two experimental protocols. The first consisted of a series of sub-

and supra-threshold rectangular current pulses of 500-ms duration applied with the stepwise increased stimulus intensity (an increment of 30–150 pA). The second protocol was a slow-ramp current injection, ramped up with a slope of 100–200 pA/s. For the recordings, V_{rest} was set at −60 mV to −70 mV by injecting a hyperpolarizing bias current, if needed. Analysis of the parameters of individual AP spikes was performed for the first AP only, at any experimental protocol applied. For the current-voltage (*I-V*) relationship for Na^+- and K^+-channel-mediated conductance, voltage-clamp recordings were consisting of voltage steps of 250-ms duration applied from –100 mV with an increment of 5 mV to 10 mV (Kopach et al., 2018a). The voltage drop (V_{drop}) during hyperpolarization was measured as the difference between the peak for a hyperpolarizing current and V_{rest} (Fig. 2A). The hyperpolarization-activated cationic current (I_h) was calculated as the sag ratio by measuring the ratio between the peak of a hyperpolarizing pulse (V_{min}) and its steady-state (V_{st}) in cell responses to −150 pA or −100 pA pulse injection as $(V_{min} – V_{st})/V_{st}$. Quantitative comparisons of the slow after-hyperpolarization (sAHP) were performed at the end of a spike train in response to a square depolarizing pulse of 500-ms duration (Fig. 2B). Clampfit 10.3 software (Molecular Devices) and Origin Pro (OriginLab, USA) were used for analysis.

Statistical analysis

Data are presented as mean ± s.e.m. with *n* referring to the number of cells analysed. The data sets not normally distributed are presented as median values. The Shapiro–Wilk test was used for testing if experimental data sets are distributed normally. For determining the statistical differences between experimental groups, one-way analysis of variance (ANOVA) with Bonferroni or Turkey multiple comparisons post-hoc test was used as appropriate. Nonparametric Mann-Whitney test or Moods median test was used to compare the medians from two or more populations. A *p* value less than 0.05 was considered as a statistically significant difference between the groups for either test used.

Funding information

This work was supported by EPSRC grant (EP/R024898/1) to AYA, the Welcome Trust Principal Fellowship (212251_Z_18_Z) and European Commission NEUROTWIN grant (857562) to DAR.

Conflict of Interest

The authors declare no conflict of interests.

Data Availability Statement

The data that support the findings of this study are available from the corresponding author upon reasonable request.

Author contributions

O.K. designed and carried out all electrophysiological experiments, analysed the data and wrote the manuscript. N.E. carried out immunocytochemistry and western blot experiments, iPSC-derived cultures. S.W. provided iPSC lines from patients. D.A.R. and A.Y.A. conceived the study and provided financial support. All authors provided editorial comments and approved the manuscript.

References

ANDRADE, R., FOEHRING, R. C. & TZINGOUNIS, A. V. 2012. The calcium-activated slow AHP: cutting through the Gordian knot. *Front Cell Neurosci,* 6**,** 47.

AZOUZ, R., JENSEN, M. S. & YAARI, Y. 1996. Ionic basis of spike after-depolarization and burst generation in adult rat hippocampal CA1 pyramidal cells. *J Physiol,* 492 (Pt 1)**,** 211-23.

BENNETT, B. D., CALLAWAY, J. C. & WILSON, C. J. 2000. Intrinsic membrane properties underlying spontaneous tonic firing in neostriatal cholinergic interneurons. *J Neurosci,* 20**,** 8493-503.

BIEL, M., WAHL-SCHOTT, C., MICHALAKIS, S. & ZONG, X. 2009. Hyperpolarization-activated cation channels: from genes to function. *Physiol Rev,* 89**,** 847-85.

BREW, H. M., HALLOWS, J. L. & TEMPEL, B. L. 2003. Hyperexcitability and reduced low threshold potassium currents in auditory neurons of mice lacking the channel subunit Kv1.1. *J Physiol,* 548**,** 1-20.

BUSCHE, M. A., WEGMANN, S., DUJARDIN, S., COMMINS, C., SCHIANTARELLI, J., KLICKSTEIN, N., KAMATH, T. V., CARLSON, G. A., NELKEN, I. & HYMAN, B. T. 2019. Tau impairs neural circuits, dominating amyloid-beta effects, in Alzheimer models in vivo. *Nat Neurosci,* 22**,** 57-64.

CRIMINS, J. L., ROCHER, A. B. & LUEBKE, J. I. 2012. Electrophysiological changes precede morphological changes to frontal cortical pyramidal neurons in the rTg4510 mouse model of progressive tauopathy. *Acta Neuropathol,* 124**,** 777-95.

CRIMINS, J. L., ROCHER, A. B., PETERS, A., SHULTZ, P., LEWIS, J. & LUEBKE, J. I. 2011. Homeostatic responses by surviving cortical pyramidal cells in neurodegenerative tauopathy. *Acta Neuropathol,* 122**,** 551-64.

DEVOS, S. L., GONCHAROFF, D. K., CHEN, G., KEBODEAUX, C. S., YAMADA, K., STEWART, F. R., SCHULER, D. R., MALONEY, S. E., WOZNIAK, D. F., RIGO, F., BENNETT, C. F., CIRRITO, J. R., HOLTZMAN, D. M. & MILLER, T. M. 2013. Antisense reduction of tau in adult mice protects against seizures. *J Neurosci,* 33**,** 12887-97.

ESTACION, M., O'BRIEN, J. E., CONRAVEY, A., HAMMER, M. F., WAXMAN, S. G., DIB-HAJJ, S. D. & MEISLER, M. H. 2014. A novel de novo mutation of SCN8A (Nav1.6) with enhanced channel activation in a child with epileptic encephalopathy. *Neurobiol Dis,* 69**,** 117-23.

ESTERAS, N., ROHRER, J. D., HARDY, J., WRAY, S. & ABRAMOV, A. Y. 2017. Mitochondrial hyperpolarization in iPSC-derived neurons from patients of FTDP-17 with 10+16 MAPT mutation leads to oxidative stress and neurodegeneration. *Redox Biol,* 12**,** 410-422.

FIEBLINGER, T., GRAVES, S. M., SEBEL, L. E., ALCACER, C., PLOTKIN, J. L., GERTLER, T. S., CHAN, C. S., HEIMAN, M., GREENGARD, P., CENCI, M. A. & SURMEIER, D. J. 2014. Cell type-specific plasticity of striatal projection neurons in parkinsonism and L-DOPA-induced dyskinesia. *Nat Commun,* 5**,** 5316.

GOEDERT, M., SPILLANTINI, M. G., JAKES, R., RUTHERFORD, D. & CROWTHER, R. A. 1989. Multiple isoforms of human microtubule-associated protein tau: sequences and localization in neurofibrillary tangles of Alzheimer's disease. *Neuron,* 3**,** 519-26.

GOTZ, J. & ITTNER, L. M. 2008. Animal models of Alzheimer's disease and frontotemporal dementia. *Nat Rev Neurosci,* 9**,** 532-44.

HU, W., TIAN, C., LI, T., YANG, M., HOU, H. & SHU, Y. 2009. Distinct contributions of Na(v)1.6 and Na(v)1.2 in action potential initiation and backpropagation. *Nat Neurosci,* 12**,** 996-1002.

HUTTON, M., LENDON, C. L., RIZZU, P., BAKER, M., FROELICH, S., HOULDEN, H., PICKERING-BROWN, S., CHAKRAVERTY, S., ISAACS, A., GROVER, A., HACKETT, J., ADAMSON, J., LINCOLN, S., DICKSON, D., DAVIES, P., PETERSEN, R. C., STEVENS, M., DE GRAAFF, E., WAUTERS, E., VAN BAREN, J., HILLEBRAND, M., JOOSSE, M., KWON, J. M., NOWOTNY, P., CHE, L. K., NORTON, J., MORRIS, J. C., REED, L. A., TROJANOWSKI, J., BASUN, H., LANNFELT, L., NEYSTAT, M., FAHN, S., DARK, F., TANNENBERG, T., DODD, P. R., HAYWARD, N., KWOK, J. B., SCHOFIELD, P. R., ANDREADIS, A., SNOWDEN, J., CRAUFURD, D., NEARY, D., OWEN, F., OOSTRA, B. A., HARDY, J., GOATE, A., VAN SWIETEN, J., MANN, D., LYNCH, T. & HEUTINK, P. 1998. Association of missense and 5'-splice-site mutations in tau with the inherited dementia FTDP-17. *Nature,* 393**,** 702-5.

IOVINO, M., AGATHOU, S., GONZALEZ-RUEDA, A., DEL CASTILLO VELASCO-HERRERA, M., BORRONI, B., ALBERICI, A., LYNCH, T., O'DOWD, S., GETI, I., GAFFNEY, D., VALLIER, L., PAULSEN, O., KARADOTTIR, R. T. & SPILLANTINI, M. G. 2015. Early maturation and distinct tau pathology in induced pluripotent stem cell-derived neurons from patients with MAPT mutations. *Brain,* 138**,** 3345-59.

IRWIN, D. J., MCMILLAN, C. T., XIE, S. X., RASCOVSKY, K., VAN DEERLIN, V. M., COSLETT, H. B., HAMILTON, R., AGUIRRE, G. K., LEE, E. B., LEE, V. M. Y., TROJANOWSKI, J. Q. & GROSSMAN, M. 2018. Asymmetry of post-mortem neuropathology in behavioural-variant frontotemporal dementia. *Brain,* 141**,** 288-301.

KIMURA, T., WHITCOMB, D. J., JO, J., REGAN, P., PIERS, T., HEO, S., BROWN, C., HASHIKAWA, T., MURAYAMA, M., SEOK, H., SOTIROPOULOS, I., KIM, E., COLLINGRIDGE, G. L., TAKASHIMA, A. & CHO, K. 2014. Microtubule-associated protein tau is essential for long-term depression in the hippocampus. *Philos Trans R Soc Lond B Biol Sci,* 369**,** 20130144.

KING, B., RIZWAN, A. P., ASMARA, H., HEATH, N. C., ENGBERS, J. D., DYKSTRA, S., BARTOLETTI, T. M., HAMEED, S., ZAMPONI, G. W. & TURNER, R. W. 2015. IKCa channels are a critical determinant of the slow AHP in CA1 pyramidal neurons. *Cell Rep,* 11**,** 175-82.

KOPACH, O. 2019. Monitoring maturation of neural stem cell grafts within a host microenvironment. *World J Stem Cells,* 11**,** 982-989.

KOPACH, O., RYBACHUK, O., KROTOV, V. & KYRYK, V. 2018a. Maturation of neural stem cells and integration into hippocampal circuits - a functional study in an in situ model of cerebral ischemia. 131.

KOPACH, O., ZHENG, K., DONG, L., SAPELKIN, A., VOITENKO, N., SUKHORUKOV, G. B. & RUSAKOV, D. A. 2018b. Nano-engineered microcapsules boost the treatment of persistent pain. *Drug Deliv,* 25**,** 435-447.

LIVESEY, F. J. 2014. Human stem cell models of dementia. *Hum Mol Genet,* 23**,** R35-9.

LOPEZ-SANTIAGO, L. F., YUAN, Y., WAGNON, J. L., HULL, J. M., FRASIER, C. R., O'MALLEY, H. A., MEISLER, M. H. & ISOM, L. L. 2017. Neuronal hyperexcitability in a mouse model of SCN8A epileptic encephalopathy. *Proc Natl Acad Sci U S A,* 114**,** 2383-2388.

LUDWIG, A., ZONG, X., JEGLITSCH, M., HOFMANN, F. & BIEL, M. 1998. A family of hyperpolarization-activated mammalian cation channels. *Nature,* 393**,** 587-91.

MATSUO, E. S., SHIN, R. W., BILLINGSLEY, M. L., VAN DEVOORDE, A., O'CONNOR, M., TROJANOWSKI, J. Q. & LEE, V. M. 1994. Biopsy-derived adult human brain tau is phosphorylated at many of the same sites as Alzheimer's disease paired helical filament tau. *Neuron,* 13**,** 989-1002.

MENKES-CASPI, N., YAMIN, H. G., KELLNER, V., SPIRES-JONES, T. L., COHEN, D. & STERN, E. A. 2015. Pathological tau disrupts ongoing network activity. *Neuron,* 85**,** 959-66.

ORTIZ-VIRUMBRALES, M., MORENO, C. L., KRUGLIKOV, I., MARAZUELA, P., SPROUL, A., JACOB, S., ZIMMER, M., PAULL, D., ZHANG, B., SCHADT, E. E., EHRLICH, M. E., TANZI, R. E., ARANCIO, O., NOGGLE, S. & GANDY, S. 2017. CRISPR/Cas9-Correctable mutation-related molecular and physiological phenotypes in iPSC-derived Alzheimer's PSEN2 (N141I) neurons. *Acta Neuropathol Commun,* 5**,** 77.

PAONESSA, F., EVANS, L. D., SOLANKI, R., LARRIEU, D., WRAY, S., HARDY, J., JACKSON, S. P. & LIVESEY, F. J. 2019. Microtubules Deform the Nuclear Membrane and Disrupt Nucleocytoplasmic Transport in Tau-Mediated Frontotemporal Dementia. *Cell Rep,* 26**,** 582-593.e5.

PICKERING-BROWN, S. M., RICHARDSON, A. M., SNOWDEN, J. S., MCDONAGH, A. M., BURNS, A., BRAUDE, W., BAKER, M., LIU, W. K., YEN, S. H., HARDY, J., HUTTON, M., DAVIES, Y., ALLSOP, D., CRAUFURD, D., NEARY, D. & MANN, D. M. 2002. Inherited frontotemporal dementia in nine British families associated with intronic mutations in the tau gene. *Brain,* 125**,** 732-51.

POORKAJ, P., BIRD, T. D., WIJSMAN, E., NEMENS, E., GARRUTO, R. M., ANDERSON, L., ANDREADIS, A., WIEDERHOLT, W. C., RASKIND, M. & SCHELLENBERG, G. D. 1998. Tau is a candidate gene for chromosome 17 frontotemporal dementia. *Ann Neurol,* 43**,** 815-25.

POWER, J. M., WU, W. W., SAMETSKY, E., OH, M. M. & DISTERHOFT, J. F. 2002. Age-related enhancement of the slow outward calcium-activated potassium current in hippocampal CA1 pyramidal neurons in vitro. *J Neurosci,* 22**,** 7234-43.

RADZICKI, D., LIU, E., DENG, H. X., SIDDIQUE, T. & MARTINA, M. 2016. Early Impairment of Synaptic and Intrinsic Excitability in Mice Expressing ALS/Dementia-Linked Mutant UBQLN2. *Front Cell Neurosci,* 10**,** 216.

ROHRER, J. D., LASHLEY, T., SCHOTT, J. M., WARREN, J. E., MEAD, S., ISAACS, A. M., BECK, J., HARDY, J., DE SILVA, R., WARRINGTON, E., TROAKES, C., AL-SARRAJ, S., KING, A., BORRONI, B., CLARKSON, M. J., OURSELIN, S., HOLTON, J. L., FOX, N. C., REVESZ, T., ROSSOR, M. N. & WARREN, J. D. 2011. Clinical and neuroanatomical signatures of tissue pathology in frontotemporal lobar degeneration. *Brain,* 134**,** 2565-81.

SHI, Y., KIRWAN, P. & LIVESEY, F. J. 2012a. Directed differentiation of human pluripotent stem cells to cerebral cortex neurons and neural networks. *Nat Protoc,* 7**,** 1836-46.

SHI, Y., KIRWAN, P., SMITH, J., ROBINSON, H. P. & LIVESEY, F. J. 2012b. Human cerebral cortex development from pluripotent stem cells to functional excitatory synapses. *Nat Neurosci,* 15**,** 477-86, s1.

SPOSITO, T., PREZA, E., MAHONEY, C. J., SETO-SALVIA, N., RYAN, N. S., MORRIS, H. R., ARBER, C., DEVINE, M. J., HOULDEN, H., WARNER, T. T., BUSHELL, T. J., ZAGNONI, M., KUNATH, T., LIVESEY, F. J., FOX, N. C., ROSSOR, M. N., HARDY, J. & WRAY, S. 2015. Developmental regulation of tau splicing is disrupted in stem cell-derived neurons from frontotemporal dementia patients with the 10 + 16 splice-site mutation in MAPT. *Hum Mol Genet,* 24**,** 5260-9.

VAN DAM, D. & DE DEYN, P. P. 2006. Drug discovery in dementia: the role of rodent models. *Nat Rev Drug Discov,* 5**,** 956-70.

VAN DER JEUGD, A., HOCHGRAFE, K., AHMED, T., DECKER, J. M., SYDOW, A., HOFMANN, A., WU, D., MESSING, L., BALSCHUN, D., D'HOOGE, R. & MANDELKOW, E. M. 2012. Cognitive defects are reversible in inducible mice expressing pro-aggregant full-length human Tau. *Acta Neuropathol,* 123**,** 787-805.

VERHEYEN, A., DIELS, A., REUMERS, J., VAN HOORDE, K., VAN DEN WYNGAERT, I., VAN OUTRYVE D'YDEWALLE, C., DE BONDT, A., KUIJLAARS, J., DE MUYNCK, L., DE HOOGT, R., BRETTEVILLE, A., JAENSCH, S., BUIST, A., CABRERA-SOCORRO, A., WRAY, S., EBNETH, A., ROEVENS, P., ROYAUX, I. & PEETERS, P. J. 2018. Genetically Engineered iPSC-Derived FTDP-17 MAPT Neurons Display Mutation-Specific Neurodegenerative and Neurodevelopmental Phenotypes. *Stem Cell Reports,* 11**,** 363-379.

WAGNON, J. L., BARKER, B. S., OTTOLINI, M., PARK, Y., VOLKHEIMER, A., VALDEZ, P., SWINKELS, M. E. M., PATEL, M. K. & MEISLER, M. H. 2017. Loss-of-function variants of SCN8A in intellectual disability without seizures. *Neurol Genet,* 3**,** e170.

WILSON, C. J. & GOLDBERG, J. A. 2006. Origin of the slow afterhyperpolarization and slow rhythmic bursting in striatal cholinergic interneurons. *J Neurophysiol,* 95**,** 196-204.

WYKES, R. C., HEEROMA, J. H., MANTOAN, L., ZHENG, K., MACDONALD, D. C., DEISSEROTH, K., HASHEMI, K. S., WALKER, M. C., SCHORGE, S. & KULLMANN, D. M. 2012. Optogenetic and potassium channel gene therapy in a rodent model of focal neocortical epilepsy. *Sci Transl Med,* 4**,** 161ra152.

Figures

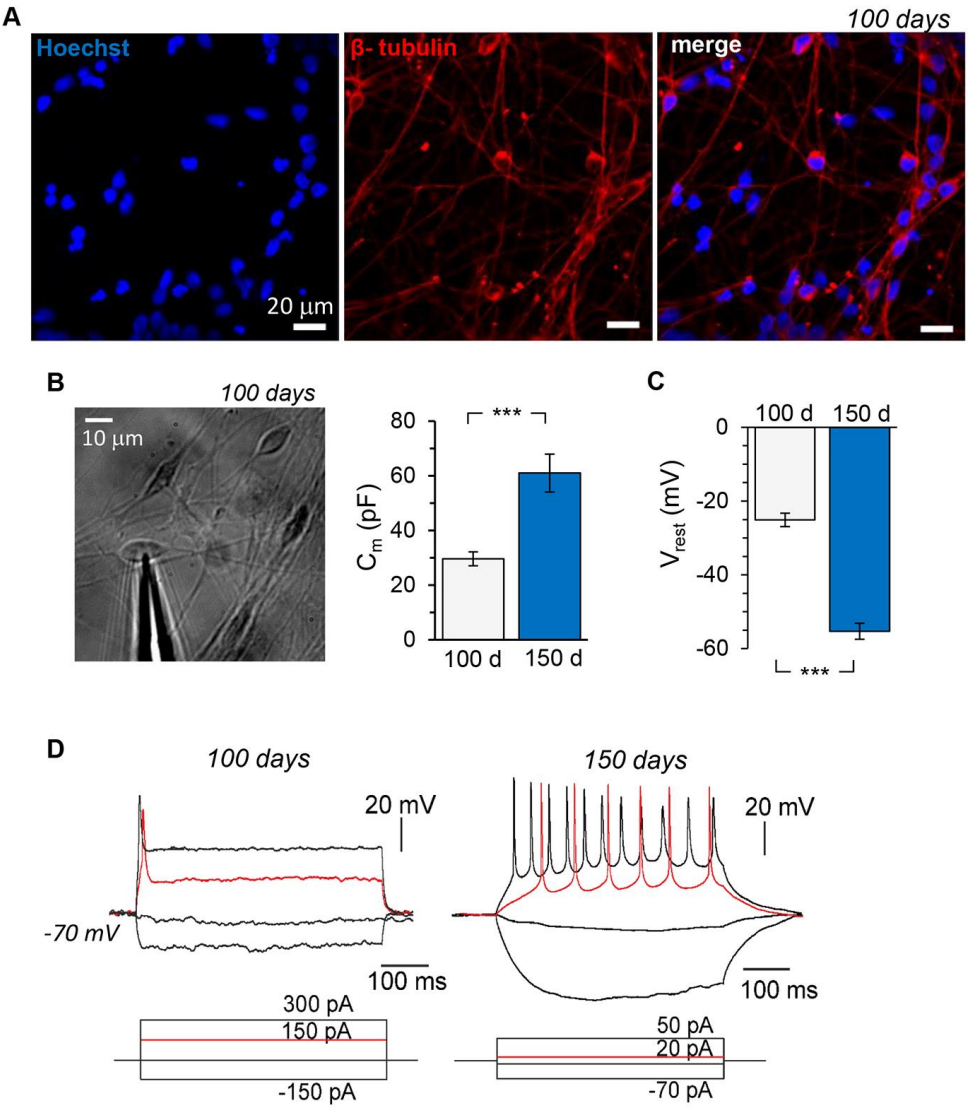

Figure 1. Time-dependent development of intrinsic excitability of human iPSC-derived cortical neurons in control (non-demented) cell lines.

(A) Immunofluorescence staining of human iPSC-derived cells for β-tubulin III (red) and Hoechst 33342 (blue), showing a clear neuronal morphology of the cells at 100 days of corticogenesis *in vitro*. Scale bars: 20 µm.

(B) Transmitted light image of human iPSC-derived neurons at 100 DIV for electrophysiological testing (left) and statistical summary of the membrane capacitance (C_m) of the cells recorded at 100 DIV (n = 17) and 150 DIV (n = 37).

(C) Statistical summary for the resting membrane potential (V_{rest}) of generated neurons at the time-points of 100 (n = 10) and 150 days (n = 23) of neurogenesis *in vitro*.

(D) Representative examples of induced firing (upper raw) by iPSC-derived neurons at the age of 100 and 150 DIV in response to injecting a series of square current pulses (indicated on the bottom). Note a high-frequency discharge induced by a current of lower stimulating intensity in a neuron at 150 DIV compared to a single AP spike elicited at the age of 100 DIV (red traces).

Data are mean with s.e.m. *$P < 0.05$; **$p < 0.001$ (ANOVA with Bonferroni post-hoc test).

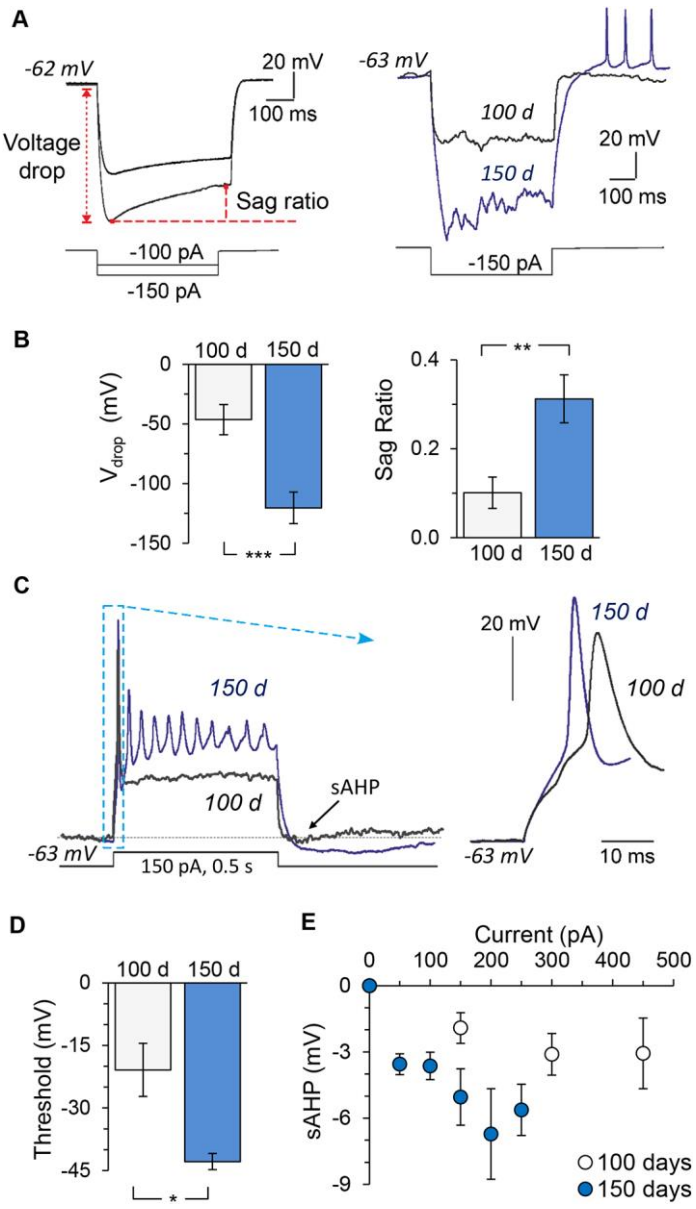

Figure 2. Time-dependent maturation of neurophysiological properties of human cells in control.

(A) Left traces, examples of patch-clamp recordings made from iPSC-derived neurons in response to a hyperpolarizing current (indicated on the bottom), depicting the way of measuring the voltage drop (V_{drop}) and the sag ratio. Right traces, an overlay of hyperpolarizing currents in responses to –150 pA by iPSC-derived neurons at the age of 100 DIV (black line) and 150 DIV (blue line).

(B) Statistical summary for the V_{drop} (left plots) and the sag ratio (right) in iPSC-derived neurons at 100 (n = 18) and 150 days (n = 17) of neurogenesis.

(C) Examples of induced firing by iPSC-derived neurons at the age of 100 DIV (black trace) and 150 DIV (blue trace), showing the slow after-hyperpolarization

(sAHP) measured at the end of prolonged (500-ms duration) square current pulse (indicated on the bottom). Box depicts the first action potential (AP) spikes illustrated on an expanded scale (right) to compare between different time-points of neuronal maturation.

(D) Statistical summary of the AP threshold in iPSC-derived neurons at 100 and 150 days of neurogenesis (n = 9 and 4, respectively). Analysis was carried out for the first AP spike elicited by injecting a slow-ramp current.

(E) Summary of the sAHP (measured as indicated in C) in response to varied depolarizing current pulses recorded in iPSC-derived neurons at 100 DIV (n = 17 cells) and 150 DIV (n = 17).

Data are mean ± s.e.m. ** $P < 0.05$; $p < 0.01$; ***$p < 0.001$ (ANOVA with Bonferroni post-hoc test).

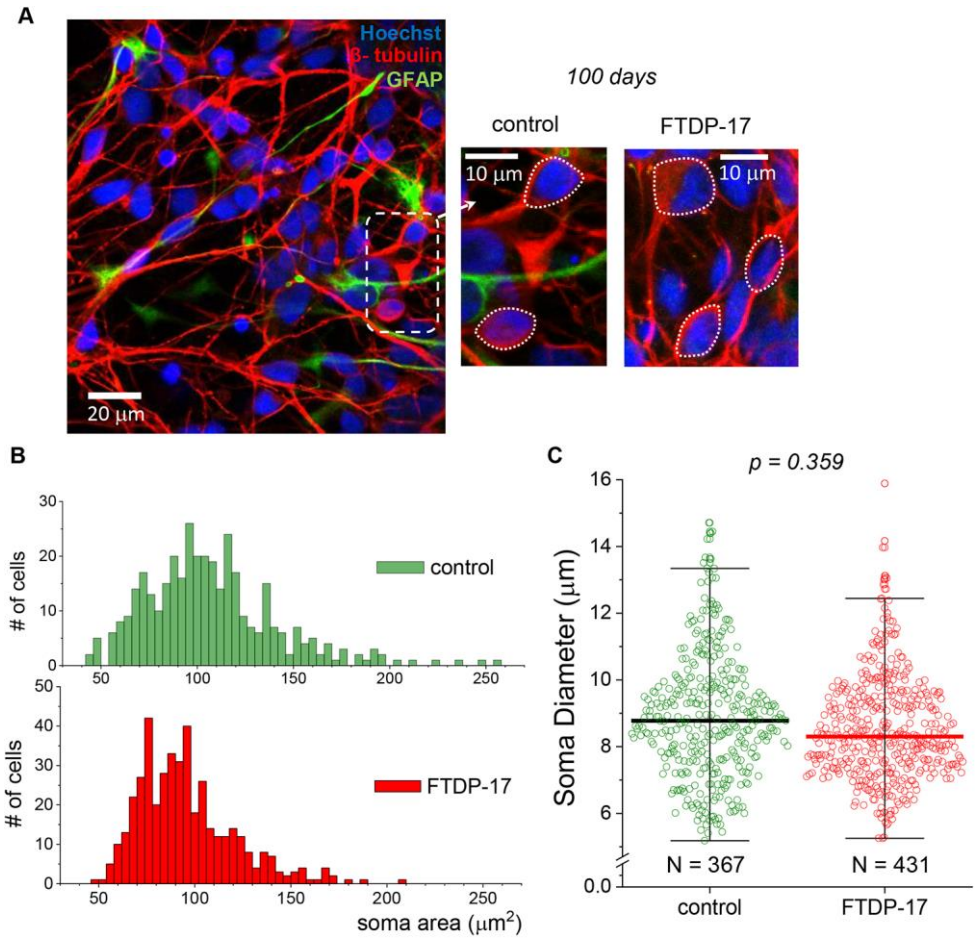

Figure 3. Similar morphological development of human iPSC-derived neurons in control and FTDP-17.

(A) Immunofluorescence staining of iPSC-derived cells for β- tubulin III (red), GFAP (green) and nuclear marker Hoechst 33342 (blue) at 100 DIV, showing neuronal morphology in a control culture (left and middle images) and one derived from FTDP patient (right image). Dotted rectangle depicts the area shown on an expanded scale; dotted circles show the way of measuring neuronal somata size.

(B) Distribution profiles of the neuronal somata area in control and FTDP-17 cultures at the age of 100 DIV (n = 367 neurons quantified in 2 control lines and n = 431 neurons in 2 cell lines from FTDP patients).

(C) Statistical summary of the neuronal soma diameter, with scatter plots showing the parameter distribution across control neurons and those with the mutation at the age of 100 DIV. Boxes show median values; the numbers of cells analysed are same as for B (nonparametric Moods median test value indicated).

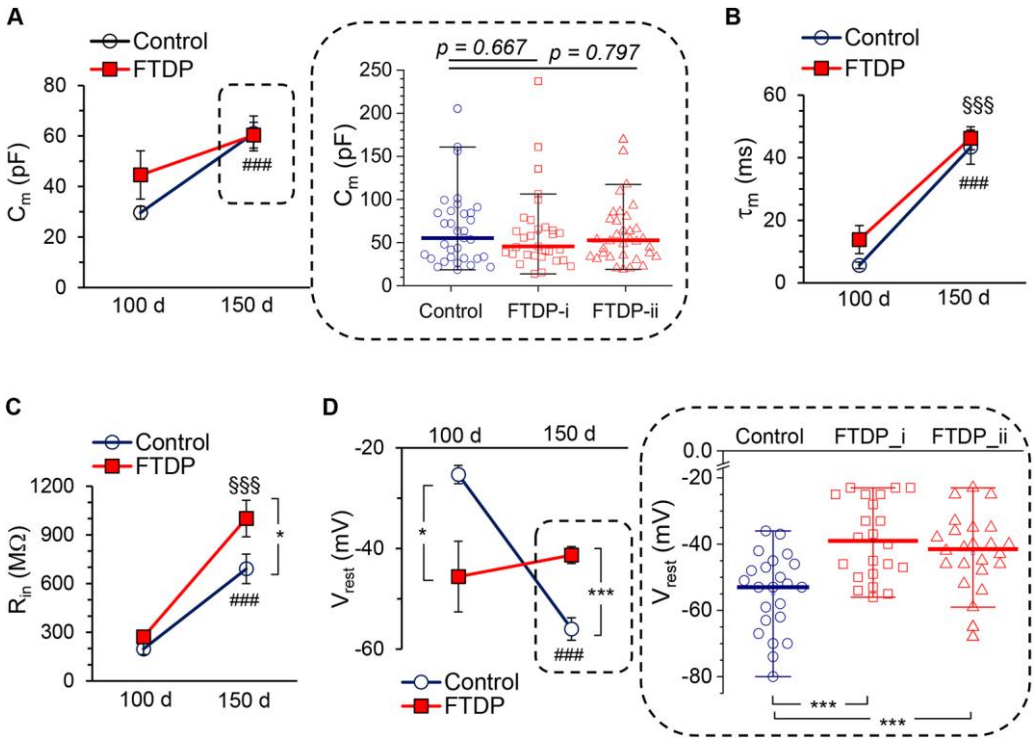

Figure 4. Human iPSC-derived neurons with tau pathology display changed passive membrane properties at an extend neurogenesis.

(A) Statistical summary of the membrane capacitance (C_m) of iPSC-derived neurons in control (non-demented group) and in cell lines obtained from two patients (FTDP-17 group) at 100 and 150 DIV. Left plots show pooled data at 100 and 150 DIV (100 DIV, n = 17 in control, n = 7 in FTDP-17; 150 DIV, n = 37 in control, n = 66 in FTDP-17). Right scatter plots demonstrate the parameter distribution for each individual case at 150 DIV (FTDP-i, n = 32; FTDP-ii, n = 34). Lines represent median values (nonparametric Mann-Whitney test values are indicated).

(B) Statistical summary of the membrane constant (τ_m) in control neurons and with the mutation at 100 DIV (n = 17 in control, n = 7 in FTDP-17) and 150 DIV (n = 37 in control, n = 66 in FTDP-17).

(C) Same as in B, but for the input resistance (R_{in}); notations as in B.

(D) Same as for (A), but for the resting membrane potential (V_{rest}). Right, pooled data at 100 DIV (n = 10 in control, n = 5 in FTDP-17) and at 150 DIV (n = 24 in control, n = 51 in FTDP-17). Left, the scatter plots showing the parameter distribution per case at 150 DIV (FTDP-i, n = 22; FTDP-ii, n = 24). Lines represent median values. ***$P < 0.001$ (nonparametric Mann-Whitney test).

Data are mean ± s.e.m unless indicated otherwise. *P < 0.05; ***p < 0.001 (ANOVA with Bonferroni post-hoc test); $^{###}p$ < 0.001 (150 DIV vs. 100 DIV for control); $^{§§§}p$ < 0.001 (150 DIV vs. 100 DIV for FTDP-17 groups).

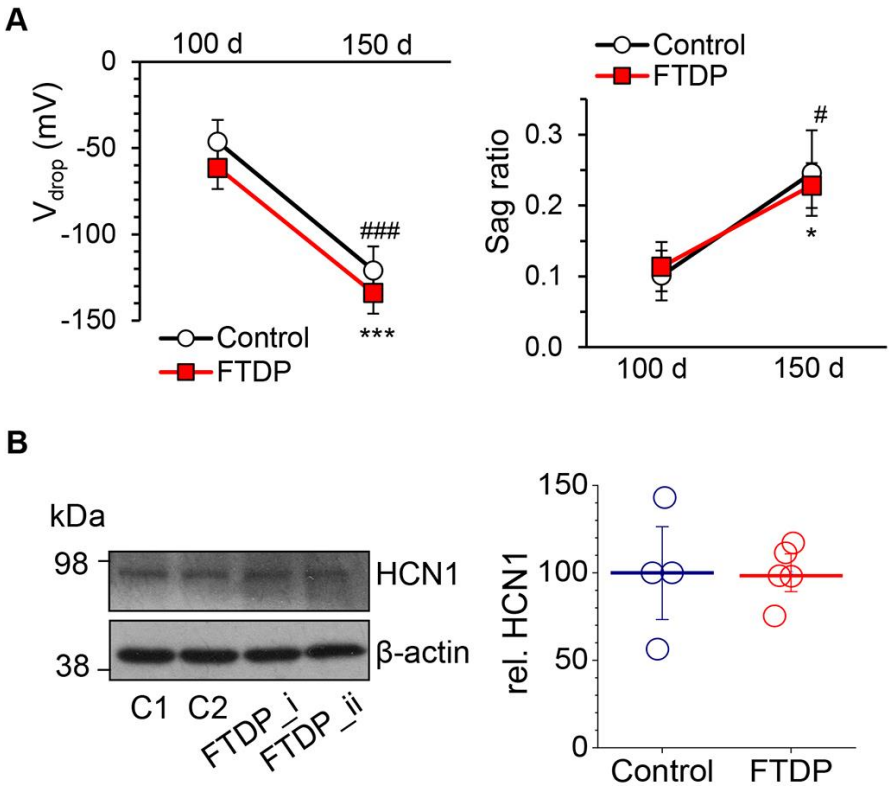

Figure 5. Time-dependent maturation of neurophysiological properties of human cells in FTDP-17: the preserved HCN-channel function at an extend neurogenesis.

(A) Summary of the voltage drop (V_{drop}, left) and the sag ratio (right) for the hyperpolarizing current pulse of −100 pA in control (non-demented) and FTDP-17 groups at 100 and 150 DIV (V_{drop}, n = 17 in control, n = 6 in FTDP-17 at 100 DIV and n = 17, n = 32 at 150 DIV, respectively; the sag ratio, n = 17 in control, n = 6 in FTDP-17 at 100 DIV and n = 16, n = 32 at 150 DIV, respectively).

(B) Left, a representative western blot for the HCN1 in iPSC-derived neurons in 2 control lines (c1-c2) and 2 FTDP-17 lines at 150-165 DIV. β-actin is loading control. Right, statistical summary for the HCN1 protein level (relative for β-actin) in control and FTDP-17 (n = 4 samples in control and n = 5 in FTDP-17, 3 independent experiments performed). Lines depict median values.

Data are mean ± s.e.m unless indicated otherwise. *P < 0.05; ***p < 0.001 (150 DIV vs. 100 DIV for control, ANOVA with Bonferroni post-hoc test); $^{\#}p$ < 0.05; $^{\#\#\#}p$ < 0.001 (150 DIV vs. 100 DIV for FTDP-17).

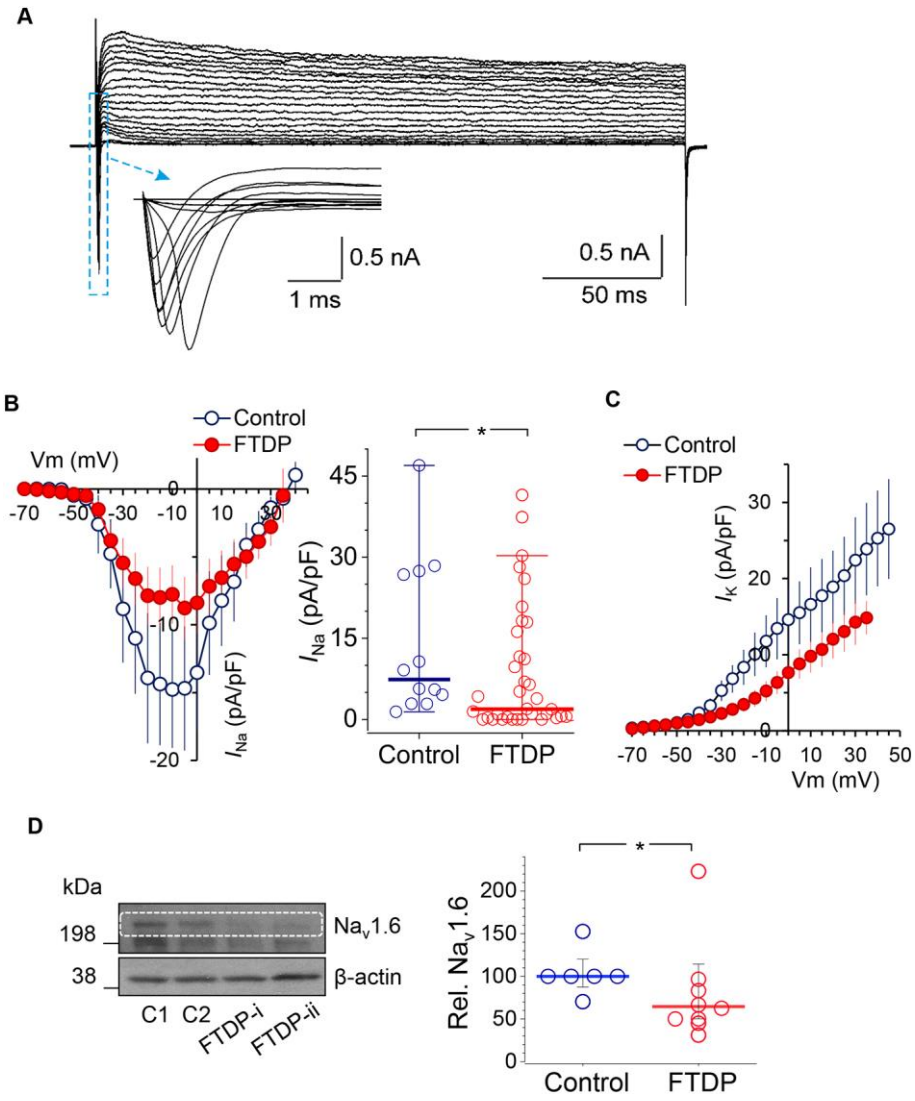

Figure 6. Tau-related down-regulation of Na^+- and K^+-channel-mediated conductance in human cells with the 10+16 *MAPT* mutation: a loss of $Na_v1.6$ channel.

(A) Example voltage-clamp recordings from a control iPSC-derived neuron at 150 DIV; box depicts the fast-activating I_{Na} on an expanded scale. The protocol consisted of voltage steps from −70 mV to +50 mV.

(B) Left plots, the current-voltage (*I-V*) relationship for Na^+-channel-mediated conductance (I_{Na}) in control cells (black) and neurons with the mutation (red) at 150 DIV; right, scatter plots of the peak I_{Na} density in control neurons (n = 12) and FTDP-17 (n = 36). Red and blue lines represent median values. *$P < 0.05$ (Mann-Whitney test).

(C) The *I-V* relationship for K^+-channel-mediated conductance (I_K) in human cells in control and FTDP at 150 DIV.

(D) The expression of $Na_v1.6$ channel in iPSC-derived neurons at 130-165 DIV in control and FTDP-17, analysed by Western blot. Left, a representative western blot including two control lines (c1-c2) and two FTDP-17 lines, with β-actin as loading control. Right, statistical summary for the $Na_v1.6$ protein level (relative to β-actin) in control (n = 6) and FTDP-17 (n = 8), obtained in 4 independent experiments. Lines depict median values. *P < 0.05 (Mann-Whitney test).

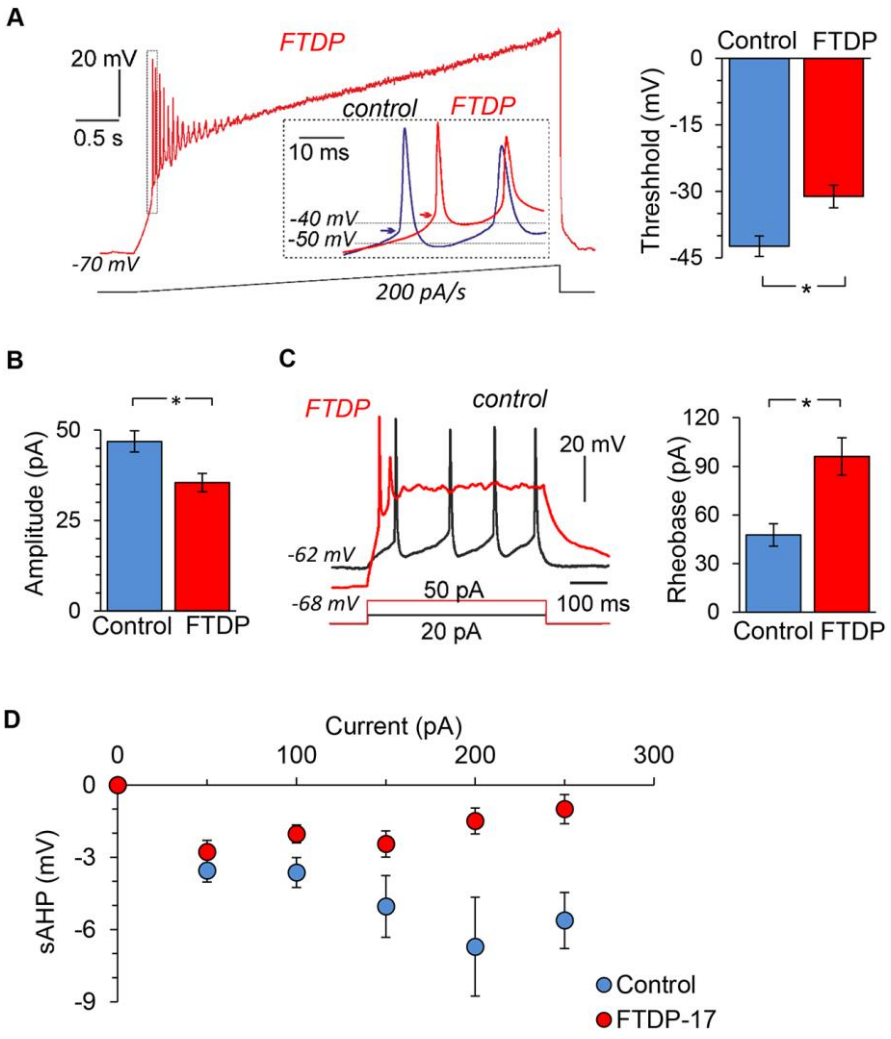

Figure 7. Phenotypic pathophysiological firing by human cells with the 10+16 *MAPT* mutation.

(A) Left, example recordings of action potential (AP) discharge by a human iPSC-derived neuron bearing the mutation (red trace) and by a control neuron (blue trace on an expanded scale) in response to injection of a slow-ramp current (indicated on bottom); dotted box illustrates the first AP spike for the analysis; insert shows overlay of expanded first AP spikes in FTDP-17 vs. control; arrows point the AP threshold. Right, summary of the AP threshold in control neurons and those with the mutation at 150 DIV (analysis performed for the first AP spike as notated on right; n = 9).

(B) Statistical summary of the AP spike amplitude in control neurons (n = 14) and neurons with the mutation (n = 36).

(C) Right, examples of firing discharge induced by square depolarizing currents (indicated on the bottom) in a control neuron (black) and neuron with the

mutation (red). Left, summary of the rheobase in control (n = 13) and FTDP-17 (n = 41).

(D) Summary of the slow after-hyperpolarization (sAHP) in iPSC-derived neurons in control (non-demented) and FTDP-17 groups (n = 15 and 32, respectively).

Data are mean ± s.e.m. *P < 0.05 (ANOVA with Bonferroni post-hoc test).